J. Fluid Mech. (1997), *vol.* 352, *pp.* 177–204. Printed in the United Kingdom

© 1997 Cambridge University Press

The shape, stability and breakage of pendant liquid bridges

By J. F. PADDAY[1], G. PÉTRÉ[2], C. G. RUSU[2], J. GAMERO[3] AND G. WOZNIAK[3]

[1] Nether Crutches, Jordans, Beaconsfield, Bucks HP9 2TA, UK

[2] Université Libre de Bruxelles, Microgravity Research Centre, Av. F. D. Roosevelt 50, B-1050 Brussels, Belgium

[3] Technische Universität Bergakademie Freiberg, Lampadiusstr. 2, D-09596 Freiberg (Sachs), Germany

(Received 24 April 1996 and in revised form 6 June 1997)

Pendant liquid bridges are defined as pendant drops supporting a solid axisymmetric endplate at their lower end. The stability and shape properties of such bridges are defined in terms of the capillary properties of the system and of the mass and radius of the lower free-floating endplate. The forces acting in the pendant liquid bridge are defined exactly and expressed in dimensionless form. Numerical analysis has been used to derive the properties of a given bridge and it is shown that as the bridge grows by adding more liquid to the system a maximum volume is reached. At this maximum volume, the pendant bridge becomes unstable with the length of the bridge increasing spontaneously and irreversibly at constant volume. Finally the bridge breaks with the formation of a satellite drop or an extended thread. The bifurcation and breakage processes have been recorded using a high-speed video camera with a digital recording rate of up to 6000 frames per second. The details of the shape of the bridge bifurcation and breakage for many pendant bridge systems have been recorded and it is shown that satellite drop formation after rupture is not always viscosity dependent. Bifurcation and breakage in simulated low gravity demonstrated that breakage was very nearly symmetrical about a plane through the middle of the pendant bridge.

1. Introduction

A pendant bridge is defined here as a system in which a section of a pendant drop supports a free hanging rotationally symmetric endplate at its lower end. Such a pendant bridge and the pendant drop shape from which it was formed are shown in figure 1. It is produced and supported by a flat circular plate or syringe tip with a centrally located hole through which liquid is introduced into the bridge. The lower end of the drop supported a circular plate of a suitable diameter, which in these experiments was the same as the tip diameter. To this lower plate was attached a rod and a second plate that lowered the centre of gravity of the endplate, so as to provide additional symmetric stability. The pendant bridge differed from other types of liquid bridges in that the force on the lower end was constant and the plate itself non-deformable.

Four types of liquid bridge systems are known and their forms are shown in figure 2. They are designated here as: (*a*) a fixed-endplate liquid bridge; (*b*) a floating-endplate liquid bridge that here we call a pendant bridge; (*c*) a rod-in-free-surface liquid bridge that is sometimes called a meniscus; and (*d*) the small bridge associated

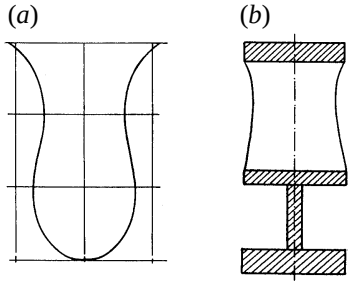

FIGURE 1. (*a*) Pendant drop ($C = -0.46$), and (*b*) an associated liquid bridge on the same scale.

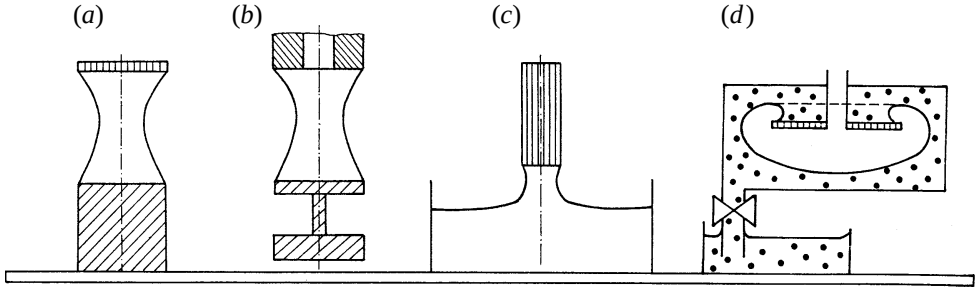

FIGURE 2. Types of pendant and sessile liquid bridges: (*a*) fixed endplate, (*b*) floating lower endplate, (*c*) rod in free surface, (*d*) sessile bubble.

with sessile bubbles. The pendant bridges of this study were constrained by two solid surfaces the lower one of which was free floating. It will be shown that as the weight of the pendant lower endplate was relatively small, the pendant bridge could be modelled as part of a pendant drop as in figure 1.

The properties of the fixed-endplate liquid bridge systems have been studied extensively by Plateau (1873), Bouasse (1922), Padday & Pitt (1972, 1973) and Meseguer & Sanz (1985) and, more recently, by Zhang, Padgett & Basaran (1996) and others. The rod-in-free-surface pendant bridge has been studied previously by Huh & Scriven (1969), and Padday, Pitt & Pashley (1975), and will not be considered further. The sessile bubble liquid bridge is usually considered as a liquid bridge without recourse to the profile from which it is derived and though relevant to pendant bridges of this study when the floating endplate is relatively heavy, will not be considered in detail here. The floating-endplate pendant liquid bridge has not been extensively studied though some previous investigations have been reported by Pétré & Wozniak (1986*a*, *b*).

Consider a pendant liquid bridge such as that shown in figure 1 (*b*), the liquid volume of which is sufficiently low for the bridge to retain stability indefinitely. When further small additions of liquid are made the bridge approaches a point of instability and at some critical volume it breaks away in a manner rather similar to a pendant drop. The bifurcation and breakage of the liquid forming the bridge takes place very rapidly and requires a high-speed camera to record the process. A part of this study was to follow these processes experimentally.

The breakaway of liquid drops issuing from an orifice and the breakup of liquid jets has been studied widely from the pioneering work of Rayleigh (1878, 1880) to the present time. Edgerton, Hauser & Tucker (1937) were the first to create experimentally a time-expanded record of pendant drop breakaway. They showed conclusively that a

satellite drop was formed from the double breakage of the neck region. The evolutionary stages of bifurcation were shown to occur within a few tenths of a second and once a cylindrical neck was formed, breakage occurred within 10^{-3} s or less. Peregrine, Shoker & Syman (1990) obtained higher time resolution by taking photos of a series of pendant drops at different interval times measured from the start of drop movement, using a single strobe flash in a darkened room. J. F. Padday (1972, unpublished data), using an ultra-high-speed ciné camera that followed a single drop through the whole evolutionary process, confirmed their findings.

Zhang & Basaran (1995) studied the breakage of a pendant drop in a normal gravity field using a Kodak high-speed camera, and recorded the breakup of a pendant drop that was continuously fed with further liquid during the course of bifurcation and breakage. Though their point of critical stability was not characterized either as a critical drop volume or a critical point in time, it appeared from their figure 7 that a marked change in the gradient of the length evolution occurred about 40 ms before breakage. The flow rate indicated that the drop volume increased by about 1 % during the bifurcation process. The neck region of their experiments elongated and broke in a manner determined by the viscosity of the liquid forming the drop. Like Edgerton *et al*. they showed that the neck region formed a satellite drop very similar to the satellite drops formed during the breakup of a moving jet of liquid. In their study, Zhang & Basaran (1995) used the total length of the pendant drop to monitor the course of the bifurcation and breakage as a function of negative time counted back from the instant of breakage. In some experiments they introduced the surface-active solute Triton X 100 suggesting that time-dependent surface tension may change the physics of breakage.

A number of theoretical treatments of the bifurcation and breakage of pendant drops have been made more recently, and notable are the studies of Schulkes (1994) and of Eggers (1995). They provide model shapes of the neck region that can be compared with experiment. The pinch-off point in Eggers' model occurred in finite time with solutions of the Stokes–Navier equation applying both before and after the singularity. The studies of Keller & Miksis (1983) of the breakup of inviscid liquid threads preceded that of Eggers and provided a self-similar description of the break point. Papageorgiou (1995) also provided a similarity solution for the breakup of a liquid jet with dynamic data suitable for comparison with experimental data.

The breakage of liquid bridges in the study by Meseguer (1983) in zero gravity was treated as a one-dimensional system that followed more the type of instability found with liquid jets than the pendant bridges of this study. Bifurcation and breakage of fixed-endplate liquid bridges show remarkable similarities to the behaviour of drops as shown by Zhang *et al*. (1996). However, under some conditions, satellite drops were not formed because breakage occurred at the lower end of the neck only, and the liquid forming the neck region was drawn upward into the upper zone.

The bifurcation and breakage have been studied by Brenner, Shi & Nagel (1994), Shi, Brenner & Nagel (1994) and Wilson (1988). These studies suggest that at very high viscosities the bifurcation process takes place much more slowly and in some instances disproportionation rather than breakage took place. Thus the threads of Shi *et al*. (1994) showed a stepwise thinning without breakage at the lower end. Brenner *et al*. (1994) demonstrated blobs along a thinning thread during the bifurcation process.

In the generalized treatment of a pendant bridge in a gravity field, the forces at equilibrium acting in a horizontal section passing through the pendant bridge must balance the free hanging liquid below that surface. It has been demonstrated theoretically by Padday (1963) that all forces acting in a horizontal section of a pendant

or sessile drop, which must include surface pressure forces, are balanced solely by surface tension forces. The omission of the surface pressure term has been suggested but is erroneous.

This study is organized into eight parts: this introduction; a theoretical part setting out the energies that operate in a pendant bridge, its associated free energy and equilibria conditions; a theoretical description of the mechanical forces that determine the stability; a method for extracting computer-generated critical equilibria data; a description of the experimental set-up and of the materials used; a comparison of computed bridge profiles with those derived from experiment; an experimental section describing bifurcation, breakage and satellite drop formation of bridges generated in normal gravity and in simulated low gravity; and finally a discussion section.

2. The shape, energy and stability properties of a pendant liquid bridge

The energy of a pendant bridge may be set out in the following way. Let V_b be the volume of the bridge, S_b its liquid–air surface area, Z_b its total length, Z_m the vertical distance of the centre of mass of the floating endplate from its top surface, Z_{cg} the position of the liquid centre of mass and E_b the energy of the bridge. The total energy of the system is given by

$$E_b = \sigma \int \partial S + \int \partial V \rho g Z + Mg(Z_m + Z_b), \tag{1}$$

where σ is the interfacial tension, ρ is the relative density of the bridge in relation to the surrounding fluid, g the terrestrial gravitational acceleration (981.1 cm s^{-2}), M the mass of the lower endplate when dry.

Equation (1) expressed in integrated form becomes

$$E_b = \sigma S_b + V_b \rho g Z_{cg} + Mg(Z_m + Z_b). \tag{2}$$

The terms on the right-hand side represent surface energy, the gravity potential of the liquid forming the bridge and the gravity potential of the floating endplate respectively.

The conditions for stable, critical and unstable equilibria are

$$\text{stable} \quad \partial E_b/\partial Z = 0 \quad \text{and} \quad \partial^2 E_b/\partial Z^2 = +\text{ve}, \tag{3}$$

$$\text{critical} \quad \partial E_b/\partial Z = 0 \quad \text{and} \quad \partial^2 E_b/\partial Z^2 = 0, \tag{4}$$

$$\text{unstable} \quad \partial E_b/\partial Z = 0 \quad \text{and} \quad \partial^2 E_b/\partial Z^2 = -\text{ve}. \tag{5}$$

The condition for non-equilibrium is

$$\partial E_b/\partial Z \neq 0 \tag{6}$$

where ∂Z represents a small reversible perturbation of bridge length.

The perturbation of the pendant bridge by a small momentary increase of Z_b at constant volume provides a suitable test for equilibrium and stability. Thus if the bridge is elongated then the restoring force upwards should increase for the bridge to be deemed stable. Were the force to decrease, then the bridge would be unstable. Here this simple perturbation is used because it is the perturbation most likely to occur in experiment and also because it is believed to be the perturbation of lowest energy and therefore the most damaging.

The shape of a pendant liquid bridge at equilibrium in a gravitational field is represented by X expressed as a function of Z, and satisfying the local equilibrium given by

$$\frac{\partial^2 Z/\partial X^2}{(1+(\partial Z/\partial X)^2)^{3/2}} + \frac{\partial Z/\partial X}{X(1+(\partial Z/\partial X)^2)^{1/2}} = (Z_o + Z)/k^2, \tag{7}$$

where Z is the axial and X the radial coordinate, Z_o, the hydrostatic height or depth of the origin of the pendant drop and k is the capillary length given by

$$k^2 = \sigma/\rho g. \tag{8}$$

Equation (7) is Laplace's capillary equation describing the equilibrium between hydrostatic pressure and the sum of principal curvatures of the liquid–fluid interface.

Bashforth & Adams (1883) have expressed the shape of a pendant drop by the dimensionless ratio, C, given by

$$C = (b/k)^2, \tag{9}$$

where b is the principal radius of curvature of the surface at the origin of the pendant drop shape. Laplace's capillary equation (7) is more readily understood in its experimental form:

$$b/R_v + b/R_h = C(Z_o + Z)/b, \tag{10}$$

where R_v and R_h are the principal radii of curvature, the former in the vertical plane and the latter in a plane at right angles to R_v. Their associated curvatures form the left-hand-side terms of (7). Thus equation (10) is equation (7) with k replaced by C and b using equation (9).

Equation (7) cannot be integrated in closed form, therefore a numerical method must be used to create drop shapes and to extract geometric properties from them. In this study fourth-order Runge–Kutta integration with a floating argument was used to create the shape data of the bridges. Details of this modelling are presented below in §4 with further details in the Appendix.

3. The equilibrium of forces acting in a pendant bridge

Consider the pendant liquid bridge system shown in figure 3, with its floating lower endplate located either at position (i) or (ii). The upper endplate, located at (iii), has a central hole through which liquid is introduced or extracted. The lower endplate consists of two small circular plates connected by a rod, which was made of aluminium or another rigid light material that was readily wetted, as shown in figure 2(*b*).

Let the radii of the wetted area of each of the two endplates be equal to X_r cm.

Making the heuristic assumption that the mass of liquid, V_l, cut off by the lower endplate exactly balances the mass of the lower endplate when hanging free gives

$$M/\rho = V_l. \tag{11}$$

Now consider the forces acting in any horizontal plane passing through the pendant bridge. Here the plane to be considered has been drawn through the wetted surface of the lower floating endplate, as seen in figure 3. The convention used here is that forces in the liquid bridge acting upwards are positive and forces acting downwards are negative.

The total effective force, F, acting on the lower endplate is given by

$$F = 2\pi\sigma X_r \sin\theta - \pi X_r^2 \sigma(1/R_v + 1/R_h) - Mg. \tag{12}$$

The first term on the right-hand side is the force due to surface tension and the second is the consequence of surface pressure arising from the curvature of the liquid surface, where θ is angle of the radius R_h to the vertical axis.

At thermodynamic equilibrium (effectively mechanical equilibrium for isothermal conditions), the resultant force, F, is zero so that equation (12) may be rewritten as

$$\frac{2\pi\sigma\sin\theta}{X_r^2} - \frac{\pi\sigma(1/R_v + 1/R_h)}{X_r} - \frac{Mg}{X_r^3} = 0. \tag{13}$$

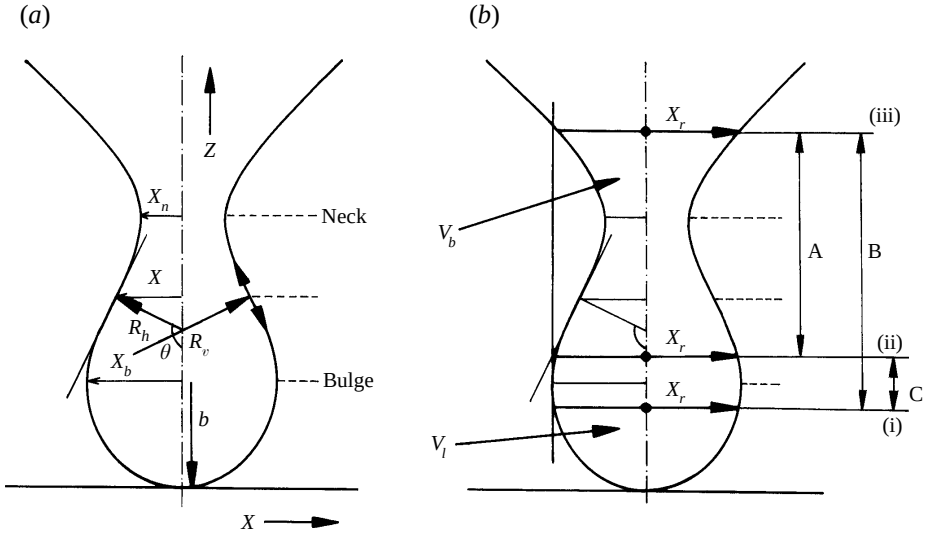

FIGURE 3. (*a*) Geometric features of a pendant bridge ($C = -0.34$).
(*b*) Pendant bridges of plate radius X_r: A and C stable and B unstable.

The capillary length k is now introduced to replace, where possible, the surface tension, liquid density and gravitational acceleration, so that

$$\frac{M}{\rho X_r^3} = 2\pi \sin\theta \frac{k^2}{X_r^2} - \frac{\pi(k/R_v + k\sin\theta/X_r)k}{X_r}. \tag{14}$$

Equation (14) is expressed in dimensionless form with X_r used as unit length. It is now combined with equation (11) to give

$$\frac{V_l}{X_r^3} = \frac{M}{\rho X_r^3} = 2\pi \sin\theta \frac{k^2}{X_r^2} - \frac{\pi k(k/R_v + k\sin\theta/X_r)}{X_r}. \tag{15}$$

It must be remembered that V_l is the excluded volume and is not an experimentally determined quantity. The volume of the pendant liquid bridge V_b is that determined experimentally.

Equation (15) is expressed in a form related to the physical forces acting in a horizontal plane passing through the junction between the liquid and the floating endplate, and may be simplified considerably using the definition of k in equation (8) to give

$$M/\pi\rho k^2 X_r = \sin\theta - X_r/R_v, \tag{16}$$

where all the experimental parameters other than X_r are moved to the left-hand side. Once these parameters are fixed either term on the right-hand side determines the equilibrium shape of the liquid bridge above this boundary condition.

We may now distinguish several special conditions. In equation (16) both R_v and ρ may be positive or negative. Also, not all pendant bridges are represented by the shape of a portion of the profile of a pendant drop. Though beyond the scope of this study, other pendant bridge shapes may be extracted from types of menisci such as the free-surface meniscus seen in figure 2(*c*) and from the neck region of captive sessile bubbles, figure 2(*d*) (Padday 1971, figure 11, curves A, B and C). Whereas the capillary pressure of bridges derived from pendant drop shapes of this study is always positive, that of bridges from free-surface menisci and from sessile bubble menisci is always negative.

The right-hand side of equation (16) is not proportional to the capillary pressure, which would be given by the sum $\sin\theta + X_r/R_v$. Instead it does give a measure of the difference between the surface tension forces and the force due to capillary pressure acting on the endplate, in dimensionless units.

The shapes of the volume of the pendant bridge are determined by the boundary conditions of the lower endplate that are fixed either by the value of the angle, θ, or by the curvature represented by X_r/R_v.

Three principal ranges of pendant bridge shapes are identified by the chosen value of $\sin\theta + X_r/R_v$, where X_r is always positive and is never zero or infinite. They are

Case 1: $\sin\theta + X_r/R_v > 0$, pendant shape applies and $M/\pi\rho k^2 X_r + X_r/R_v < 1$;

Case 2: $\theta = \pi/2$ and $R_v = \infty$, cylindrical bridge applies and $M/\pi\rho k^2 X_r = 1$;

Case 3: $\sin\theta + X_r/R_v < 0$, rod in free surface or sessile bubble shape applies and $M/\pi\rho k^2 X_r \gg \sin\theta$ and $-X_r/R_v > 1$.

Case 1 applies to systems where the mass of the endplate is relatively small. Case 2, the cylindrical meniscus, is a special condition of case 1. When the excluded volume of the pendant drop shape coincides exactly with the plane passing through the minimum diameter of the neck of the associated drop, such a cylindrical bridge is formed but with very small volume. Thus the endplates of cases 1 and 2 are held up by surface tension forces alone.

Pendant bridge shapes supporting relatively large endplate weights are more likely to be represented by free surface or sessile bubble shapes and are, of course, of negative capillary pressure. Under these conditions surface tension and capillary pressure act together, R_v/X_r becomes small and negative and $\sin\theta$ tends towards zero. The shapes of such pendant bridges are represented by the conditions of case 3 and have not been studied further here.

No attempt has been made in this study to model or experiment with heavy endplates where the bridge has very small volumes. However, the shapes of such very small bridges correspond to θ becoming very small so that surface tension no longer plays a significant role in supporting the endplate. Rather it is now supported principally by surface pressure acting upwards and not downwards as with the experimental pendant bridges of this study.

Let the height, Z, of a Case 3 type pendant bridge approximate to $2R_v$ so that the volume of the bridge is given by

$$V_b = \pi X_r^2 Z = 2\pi X_r^2 R_v. \tag{17}$$

When equation (17) is combined with (16) and (8) and rearranged the result is

$$\sigma = MgV_b/2\pi^2 X_r^4. \tag{18}$$

Equation (18) has been used in an attempt to measure surface tension (Pétré 1995) but it is somewhat innacurate because the assumptions are only approximate and the experimental volume, V_b, is very difficult to measure precisely.

Returning to the pendant bridge shapes of this study that are well represented by a portion of the pendant drop profile, integration is necessary to derive the bridge properties from the boundary conditions at the lower endplate, derived above.

The full shape is then obtained by integrating the Young–Laplace equation from the boundary conditions of the lower endplate until the upper endplate dimension is reached. In this study we have chosen to use pendant drop shapes to model the pendant bridge mainly because we were able to compare our data with the pendant bridge shape

extracted from the extensive tables of pendant drop shapes available in the literature (Hartland & Hartley 1976). Comparison with liquid bridge tables, where they exist, would have involved nonlinear interpolation.

4. Computer modelling of pendant bridge properties

An attempt has been made to extract the properties of pendant bridges using similar computing techniques to those that were successful with pendant drops. Figure 3(*a*) is that of a pendant drop of shape factor $C = -0.34$. Figure 3(*b*) shows three pendant bridges A, B and C that may be extracted from this given shape.

The geometric and stability properties of pendant bridges were obtained by generating the pendant drop shape, starting at the origin of the drop shape where it meets the axis of symmetry. The profile is then created from equation (10), using fourth-order Runge–Kutta as the preferred numerical method. Integration was continued until the value of V/X^3 of the pendant drop profile corresponded to that of a preselected value of $M/\rho X_r^3$ ($= V_l/X_r^3$), i.e. point (i) in figure 3(*b*). More details of this modelling method are presented in the Appendix.

When point (i) was reached, the value of X/k was recorded and integration of the shape continued until a second (ii), and third (iii) fit was reached corresponding to this same value of X/k. The properties of bridges B and C of figure 3(*b*) were then obtained as (iii)−(i) and (ii)−(i) respectively. The bridge A formed from (ii)−(iii) did not correspond to the same value of $M/\rho X_r^3$ because it cuts off a larger volume of liquid. It did however correspond to a real bridge. During the process of data extraction, it was found that the first fit to the value of $M/\rho X_r^3$ sometimes occurred above the bulge, thus only one stable bridge, A, could be found.

The properties recorded at each fit point were angle, X, Z, S, the surface area, V, R_v, R_h, F the peripheral distance from the origin and E, the energy. These properties, though used to check the validity of data, are not presented in this paper.

The extraction of pendant bridge data was continued using the same value of $M/\rho X_r^3$ with further new shapes, values of C, until a whole array of pendant bridge data were obtained for the given value of $M/\rho X_r^3$. This array of data was then normalized to a constant value of $X_r = 1$ by dividing all lengths by the corresponding values of X_r/k.

The length of the bridge, Z_b/X, of each array has been plotted as a function of V_b/X^3 in figure 4 for 8 different values of V_l/X_r^3. The values 2.7875 and 5.774 were chosen as they represented values corresponding to endplates used experimentally.

The curves of figure 4 demonstrate that the volume of a bridge grows at stable equilibrium with the length Z/k increasing at the same time. Eventually the volume of liquid in the bridge reaches some maximum value, V_c, at which point the bridge becomes unstable. The bridge then appears to stretch at constant volume, cascading through a series of non-equilibrium shapes with further increases in length until eventually the bridge breaks completely. In figure 4 an upper envelope curve has been drawn to include all Laplace shapes for such pendant bridges. Thus the irreversible stretching of the unstable bridge at constant volume was believed to continue until this envelope curve was reached.

During the early stages of stable growth the ratio Z/X_r was a measure of pendant bridge growth. The ratio V_b/X_r^3 provided a similar measure of stable growth. Even in the early stages of growth a neck was formed of diameter $2X_n$ and it was found possible to use the neck diameter as a measure of characteristic shape. Thus to compare experimental with theoretical shapes, the value of $2X_n/Z$ was determined at constant Z/X_r.

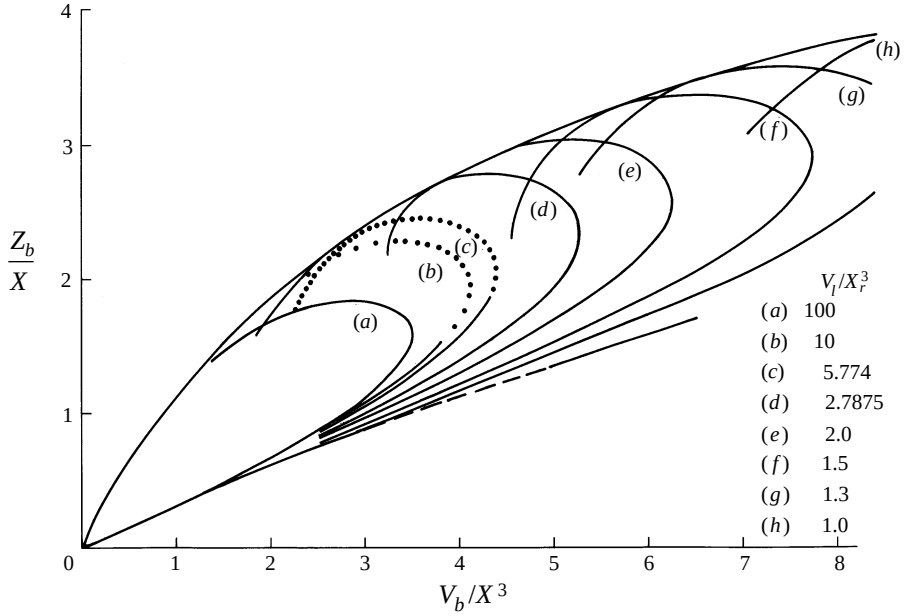

FIGURE 4. Computer-generated relationship between Z_b/X and V_b/X^3. Each curve represents the length of the pendant bridge as a function of bridge volume reduced by the radius of the endplates for a given constant value of the mass of the hanging endplate.

5. Experimental

The apparatus used to create pendant liquid bridges has been described elsewhere (Wozniak *et al.* 1993). It consisted of a microsyringe connected by a piece of microbore plastic tubing to an endplate 4.0 mm in diameter. This endplate was mounted rigidly over a cuvette consisting of a square glass cell from an absorptiometer and of 10 mm section. For our experiments, the apparatus was adapted by using a short length of Teflon tubing to connect the syringe to the glass tube forming the upper support of the pendant bridge. The lower floating endplate was mounted on a small block inside the cuvette and the whole cuvette was moved up and down by resting it on an adjustable platform. Three powerful tungsten lights were placed within 150 mm of the apparatus and a Kodak high-speed video camera mounted on a rigid tripod was located nearby.

To perform an experiment a small amount of liquid was pushed out of the syringe manually so that the upper endplate was wetted. The lower endplate was now raised towards the upper one until it touched the liquid and was just wetted. The two endplates then became attached by a very thin liquid bridge which was also self-centering. The platform was now lowered leaving the lower endplate hanging free. More liquid was now introduced and the camera focused, the lights turned on and the camera started. Still more liquid was slowly added until the bridge broke at which point the camera was immediately stopped. This dramatic stop was essential as the camera memory only secured the last second of the sequence of pictures when the camera speed was set at its maximum of 6000 frames per second. The sequence of images of the breaking drop was recorded digitally and then transferred separately, first to a record on magnetic tape and then as a direct record on a magneto-optical disk.

Each image was then entered separately into the computer memory taking care that each experimental sequence maintained constant magnification. Thereafter, a selection of images from each sequence was arranged in an array so that relative changes of

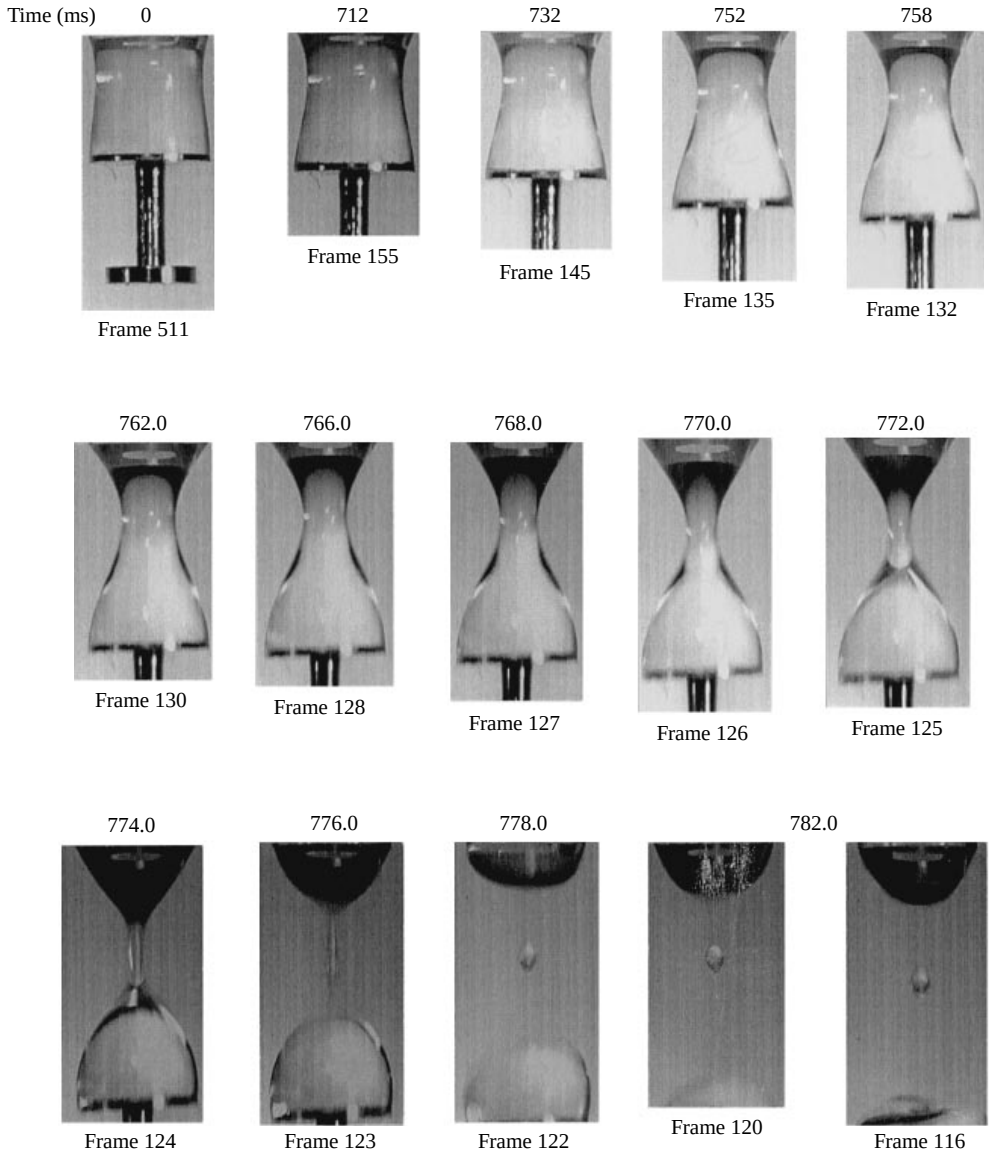

FIGURE 5. Bifurcation and breakage of a pendant bridge. The endplate radii are 2 mm and the liquid, pure water. Frame numbers and elapsed time from the first frame in the sequence are shown. Camera speed was 500 frames s^{-1}. Experiment 29/06/95, ID01.

shape and extension became apparent. Tables of the data plotted in figure 4 were prepared and printed so that interpolation of properties at maximum bridge volume were more accurate.

The array of images in figure 5 shows the results from a typical experiment. The camera was set at the relatively low speed of 500 frames s^{-1} and at this rate the image area encompassed the whole of the bridge volume. Fifteen frames have been selected from among the 5000 or so images recorded to show the progress of bifurcation and breakage of the bridge.

The weight of the floating endplate was 0.0223 g and its radius 2.00 mm. The density

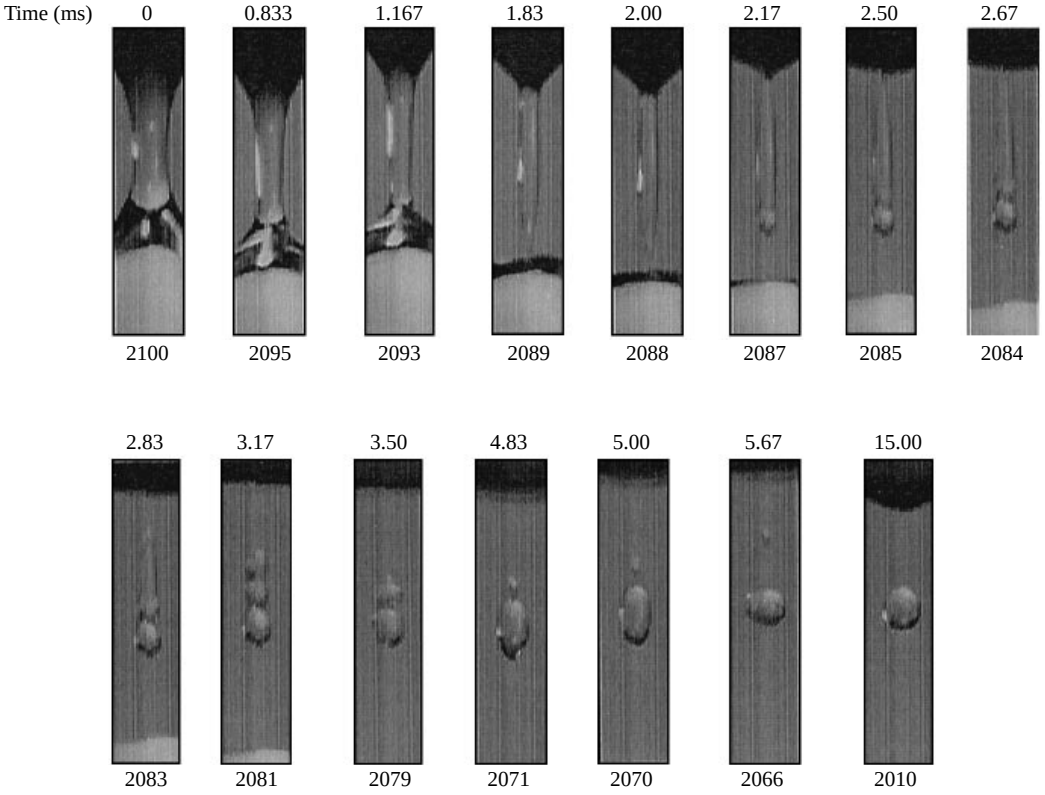

FIGURE 6. Bifurcation and breakage of a pendant bridge. Bridge composed of pure water. Video speed was 6000 frames s^{-1}. Experiment 28/06/95, ID20.

of water was taken as 0.998 g ml^{-1} and the gravitational acceleration as 9.811 m s^{-2}. Thus the value of $M/\rho X_r^3$ of equation (15) was 2.7875 amd corresponded to curve (*d*) of figure 5 and figure 7.

Between frames 124 and 122 of figure 5 breakage took place but the frame speed was insufficient to capture details of the actual breakage process. The breakage was now followed at the higher speeds of 6000 frames s^{-1} to clarify the details, which are shown in figure 6. However, the camera itself was limited in the total number of pixels per second acquirable and so modifications to the system were imposed – first the area to be recorded was greatly reduced to that actually needed, and second the total length of record was limited to less than 1 s. The resulting array of images recording the detail of breakage and satellite drop formation, shown in figure 6, were recorded in this way. The scale of size in figure 5 corresponds to a real plate diameter of 4 mm. The scale in figure 6 is not indicated, but the frame width was very near 1 mm.

Experiments with other liquids were limited to water/glycerol mixtures, with the exception of one where a solution of polyethylene oxide polymer with a molecular weight of about 4×10^{-6} was used. The solution possessed a maximum viscosity of 400 mPa s and shear thinned strongly. The water/glycerol mixtures were all Newtonian.

A few experiments were performed in a Plateau tank using two immiscible liquids of near equal density. The outer liquid was water and the bridge liquid was a mixture of dioctyl phthalate and dibutyl phthalate: approximately 68% of the former and 32% of the latter by volume. The final oil density was then adjusted to equal density with

water by adding one or other of the components until a drop of the oil of diameter 2 mm or larger remained suspended in water without rising or falling. The oil also contained a very small trace of azobenzene, a yellow dye that made the oil phase more visible.

6. Comparison of computed shape with experiment

Figure 4 shows that the height of a pendant bridge increases with bridge volume for a series of stable bridges according to the properties of the endplate and of the liquid forming the bridge. In figure 7, the height of the bridge, Z/X_r, is again shown as a function of V_b/X_r^3, for the data of curve (d) of figure 4. Five stable equilibrium bridge profiles have been plotted by the computer from a selection of points on the growth curve of the pendant bridge. These profiles are shown in figure 7 and their corresponding positions on the curve, shown as profiles (a–e). The profile of the critical equilibrium shape, (f, was generated in the same way. A further three non-equilibrium shapes, profiles (g–i) were also generated. The profiles of these nine boundary conditions were generated with the same computing program as that used to obtain the data of figure 4. Three experimental frames taken from two different experiments and printed to the same scale are included for comparison.

The last three profiles (g–i) were obtained differently. They were obtained on the basis that the force on the lower endplate was insufficient to hold it up. Thus by extracting a profile with a value of $M/\rho X_r^3$ ($= V_l/X_r^3$) slightly lower than that of the experiment, and then searching for the position with a pendant bridge volume ratio, V_b/X_r^3, equal to that at critical conditions, a non-equilibrium profile, such as F in figure 7, was generated. The purpose in doing this was to enable comparison of experimental shapes with these non-equilibrium profiles on the basis that only surface and gravitational forces were acting and that inertial forces of the liquid were insignificant.

The computed growth curve of figure 7 was very much as expected, starting with lower values of shape factor which then increase towards zero. Growth took place until the critical volume was reached at a maximum volume which is clearly seen. Matching the equilibrium profiles with experimental shapes was attempted with experimental frame 375 being modelled by profile (d); frame 155 by profile (f) which was thought to be very near critical conditions, and frame 135 by the non-equilibrium shape (g) of figure 7.

Comparison was made by first finding a computed profile with the ratio Z/X_r equal to that of the chosen experimental frame. The ratio of minimum neck diameter to length of the bridge, $2X_n/Z$, of the experiment was then compared with that of the computed profile. This ratio was found to be a very sensitive measurement of small shape changes.

A first comparison made was of frame 375 of an experiment, the array of which is not presented here, with the computed profile (d) of figure 7. The height, Z/X_r, of the experimental profile was 1.94 and that of the computed profile, 1.92. The ratio $2X_n/Z$ of profile (d) had a value of 0.95 and that for experiment frame 375 was 0.93 with a reproducibility of ± 0.02. The whole of the error lay in the imprecision of measurement of the dimensions of the experimental profile.

A further comparison of frame 155, taken from the data of figure 6, was made with the critical shape, profile (f), of figure 7. The value of Z/X_r for the experimental frame was 2.22 and for profile (f), 2.28 which was sufficiently close for comparison. The corresponding values of $2X_n/Z$ were 0.694 for the experiment and 0.682 for the computation. A further error occurred from possible imprecision of the location of the

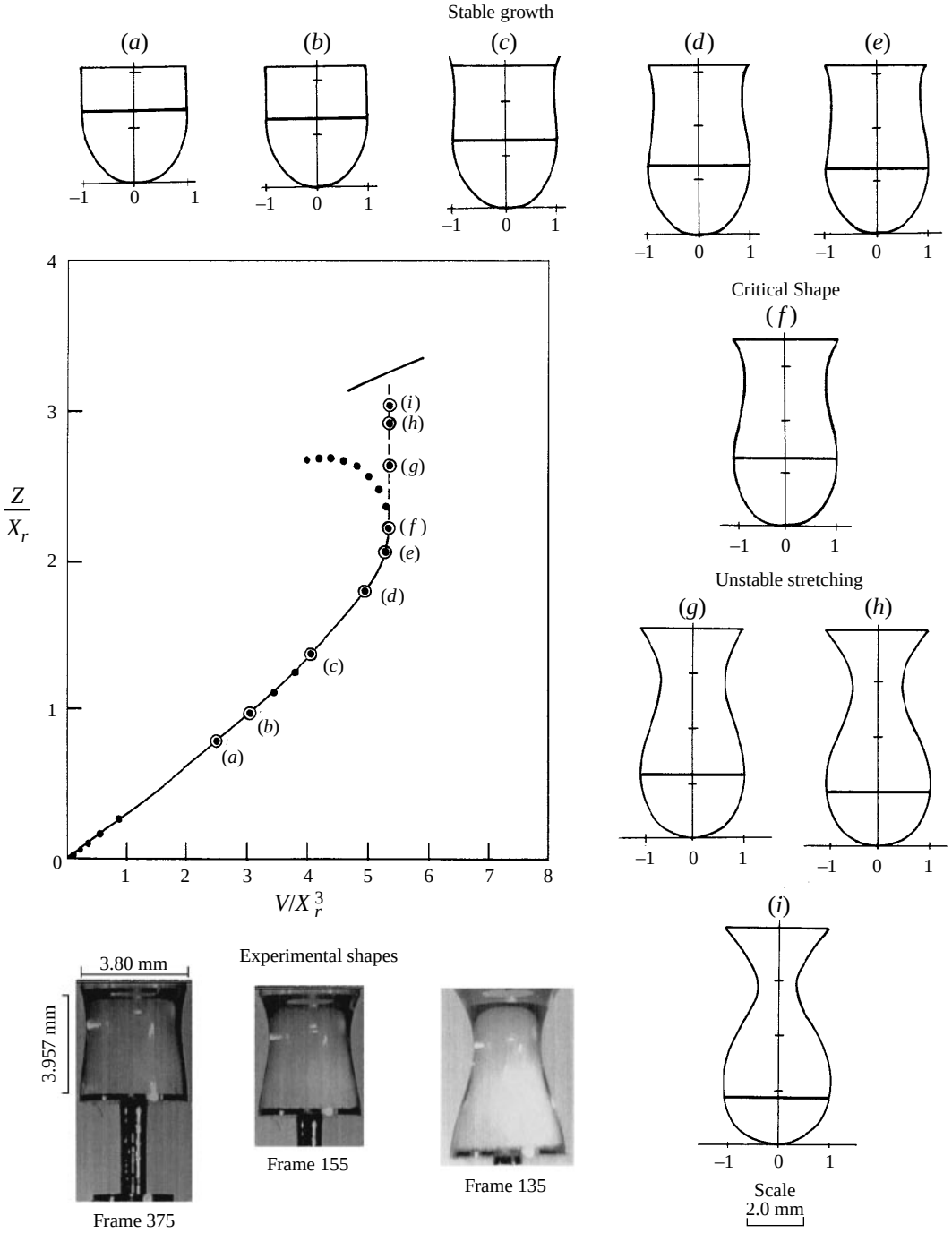

FIGURE 7. Computer-derived shapes of pendant bridges. Stable pendant bridge growth with increase in volume. Lower endplate $M/\rho X_r^3 = 2.7875$. Shape factor C is (*a*) -0.59, (*b*) -0.58, (*c*) -0.55, (*d*) -0.50, (*e*) -0.48. Shape (*f*) is the critical volume, $C = -0.46$. Shapes (*g*), (*h*) and (*i*) are unstable equilibrium shapes where $M/\rho X_r^3$ becomes 2.5, 2.0 and 1.688 respectively. Experimental frame 375 corresponds to (*d*), 155 to (*f*) and 135 to (*g*) and (*h*) respectively.

maximum computed volume. Even so, the agreement between computation and experiment is sufficiently close to provide confirmation that the critical point was represented by the position of maximum volume.

Frame 135 from figure 5 was chosen as an example of a non-equilibrium profile because the value of Z/X_r lay in the non-equilibrium region of the graph of figure 7 and was compared with the computed profile (*h*). The value of Z/X_r of the experimental profile was 2.85 and that of the computed profile, 2.98. The value of $2X_n/Z$ of frame 135 was 0.39 and that of profile (*h*) was 0.32. The poor agreement was partly due to the poor agreement of the two heights but even so the comparison suggested that the neck in the experimental frame was larger than that of the computed frame of equivalent length. Comparison of shapes in this region carries much larger errors, first because the experimental shape itself is moving more rapidly, and second because the computation method for non-equilibrium shape was not sufficiently developed to derive an exact fit to the experiment. Also the effects of inertia terms in the force balance have been omitted.

The method of comparison of experimental shape with computer-modelled shape provides very little that is new. Such comparisons have been made in the past with pendant drops and the techniques for these comparisons are well known. However the most interesting point to emerge was that the growth of these experimental pendant bridges started with a near cylindrical bridge of very small volume and height and then grew with the shape factor increasing and the neck becoming more pronounced. This growth is seen clearly from the equilibrium profiles of figure 7. The cylindrical profile of very small volume would thus approximate to the condition of case 2 of equation (16), given by $M/\pi\rho k^2 X_r = 1$, but only for this particular endplate.

7. The bifurcation and breakage of pendant bridges

Once a pendant bridge had reached the point of critical instability, point (*f*) in figure 7, further changes became irreversible and the bridge, like a pendant drop, continued to change shape until it finally broke away from its support. The sequence of irreversible shape changes that took place between the critical point and the final breakage, termed bifurcation, are shown in figure 5. The array of images in figure 5 shows that growth of the pendant bridge occurred up to frame 155 which represented critical conditions, and thereafter there was bifurcation between frames 155 and 123. Breakage took place at the lower end of the neck region first, and later at the upper end, with the liquid in the neck region forming a satellite drop in free fall. The numbers on top of each frame indicate the relative elapsed time counted from frame 511 (an arbitrary choice of starting point).

Inspection of a number of arrays of images of the bifurcation process of pendant bridges suggested that the process of irreversible movement of liquid may be broken down into three periods. These periods are shown in table 1 together with their duration in ms for two different experiments. Experiment 29/06/95 ID01 was a bridge of water alone and experiment 28/06/95 ID01 was that of a binary solution of water with 70% glycerol of much higher viscosity. The array of this latter experiment is not shown here. The timescales of the breakages from the data of figures 6 and 8 provide the higher time resolution needed to see the breakage. The large difference in the time elapsed during growth of the bridge in the two experiments reflects the arbitrary choice of starting point. Like previous experimental investigations we confirm that the bifurcation process is relatively slow, the breakage is very fast and the final recoil and associated damping of intermediate time depend on viscosity.

Process	Duration (ms) 29/06/95 Expt ID01 & 20 (figure 6) Water	28/06/95 Expt ID01 Array not shown 70% glycerol
Growth		
Equilibrium Laplace shapes	712	48
Bifurcation		
Non-equilibrium Laplace shapes	42	44
Bridge elongation and endplate acceleration	16	12
Cylindrical neck evolution	4	—
	Expt ID20 (figure 7)	Expt ID13 (figure 8)
Breakage		
Breakage of neck from lower end	< 0.1	< 0.1
Recoil of lower end of neck	0.67	0.84
Breakage of neck from upper end	< 0.1	< 0.1
Evolution of satellite drop	< 2	< 2
Recoil and stabilization	60	20

TABLE 1. Duration of bifurcation and breakage processes at pendant bridge instability

7.1. *Bifurcation of the pendant bridge*

During the initial stage of irreversible change within the pendant bridge, liquid flowed from the neck region towards both supporting surfaces accompanied by a corresponding decrease in surface energy. During this first stage of bifurcation, comparison with non-equilibrium profiles as already made in §6 is justified but is only relevant up to the point where Z/X reaches its maximum value set by the position of the enveloping curve of figures 4 and 7. In this period drop elongation took place relatively slowly as indicated in table 1 and figure 5.

Once the length of the bridge exceeded the limit fixed by the envelope curve further comparison with computed shape was not relevant. Even so, it was found that in these later stages of bifurcation the conical shape of liquid attached to the upper endplate as seen in frames 127, 126 and 125 of figure 5 matched very closely with the cone of liquid at the upper endplate of computed shape I of figure 7. This apparent agreement of cone angle between computer and experiment indicated that the conical shape, though transient, was best explained by surface forces alone. The modelling of the evolution of the profile of the pendant bridge should include inertial terms. During bifurcation, the bridge profiles of this study followed, very closely, those of normal pendant drops referred to in the introduction.

The final stage of bifurcation was the evolution of the neck region from frame 125 to frame 776 of figure 5. Changes here occurred so quickly that higher time resolution of 6000 frames s^{-1} was required to record changes as seen in figure 6. This figure shows that breakage at the lower end of the neck took place between frame 2089 and 2088. Breakage at the upper end was not so clear and occurred near to frame 2084. We observed from many experiments that the zone of liquid at each endplate relaxed within one frame to the characteristic curvature of a surface without any pimple once breakage had occurred. During this final stage the liquid forming the neck of these studies became cigar shaped.

7.2. *Bridge breakage and satellite drop formation*

Breakage of pendant drops took place first at the lower end, as shown by Peregrine *et al.* (1990) and others, and later at the upper end of the neck region of the pendant bridge. The time interval between the two breakages was less than a ms. Immediately after either breakage three types of recoil took place: first the liquid zone attached to the lower endplate recoiled to a near-spherical cap within one frame (0.166 ms); secondly, the lower end of the neck liquid moved upwards to start forming the shape that eventually became the satellite drop, as shown by Peregrine *et al.* (1990) and by Zhang & Basaran (1995); thirdly, it was quite evident from frames 2087 to 2085 of figure 6, that though the neck liquid was still attached to the upper endplate liquid, the shape of the upper half-zone had relaxed from that of a cone to that of a near-spherical cap. Breakage at the top end of the neck took place at frame 2081 and immediately the upper end of the neck liquid relaxed downward to meet that rising from the lower break. A satellite drop was formed from this neck liquid and it continued to suffer recoil pulses for another second.

In a further experiment, figure 8, the breakage of a more viscous liquid composed of 80 % glycerol in water with a viscosity of 108 mPa s was followed using the same set-up and the same camera speed of 6000 frames s^{-1}. Figure 8 shows very clearly that the processes of neck breakage and of satellite drop formation followed the same three periods but this time the breakage at each end of the neck region was very much clearer. Breakage at the lower end took place at frame 2289 and at the top end at frame 2284, a time interval of less than 1 ms and very similar to that of water. The bifurcation process at this greater viscosity was much slower. Frame 2095 of figure 6 for water, is very nearly the same shape as frame 2304 of figure 8, for the glycerol–water solution. The intervals between these frames and the lower-end breakage are 1 ms for water and 2.5 ms for the high-viscosity liquid.

The satellite drop profile of frame 2276 of figure 8 again nearly matched frame 2079 of figure 6, yet the former took 2.16 ms to reach this stage after the break of the lower end of the neck, whilst at lower viscosity the elapsed time was 1.66 ms. It appeared that the volume of each satellite drop was not very different and also the shape and lengths of the neck portions of each experiment were similar.

The bifurcation and breakage of a series of liquids covering a range of viscosities were recorded with the high-speed camera, each liquid being a mixture of glycerol and water. A further liquid that was a polyoxyethylene polymer (Mwt 4×10^{-6}) was also examined using the same technique. This polymer solution was viscoelastic and showed pronounced shear thinning properties. Bridges formed with this liquid never broke and could be stretched to as much as 200 mm and will be fully reported separately. The neck shapes at the point where the lower end broke away, for each of these liquids, are shown in figure 9. The properties of the liquids involved are also given and it may be seen that the surface tension does not vary very much, whilst the Newtonian viscosities cover a range of 108 to 1 mPa s.

It is evident that shapes of the necks of liquids A2, B, C, D, and E are all very similar as are the thicknesses at the middle of the neck. The length of the neck of the water and of liquid B at the point of breakage are about the same, whereas the neck lengths of liquids C, D and E are slightly longer. Even so, there is a suggestion that water necks are somewhat thicker and shorter than the others. Also it is evident that the length of the neck is about fifteen times the diameter of the neck, thus precluding the types of instabilities found by Plateau (1873) and by Rayleigh (1878). Further evidence that the breakage was not the outcome of Plateau- or Rayleigh-type instabilities was found by

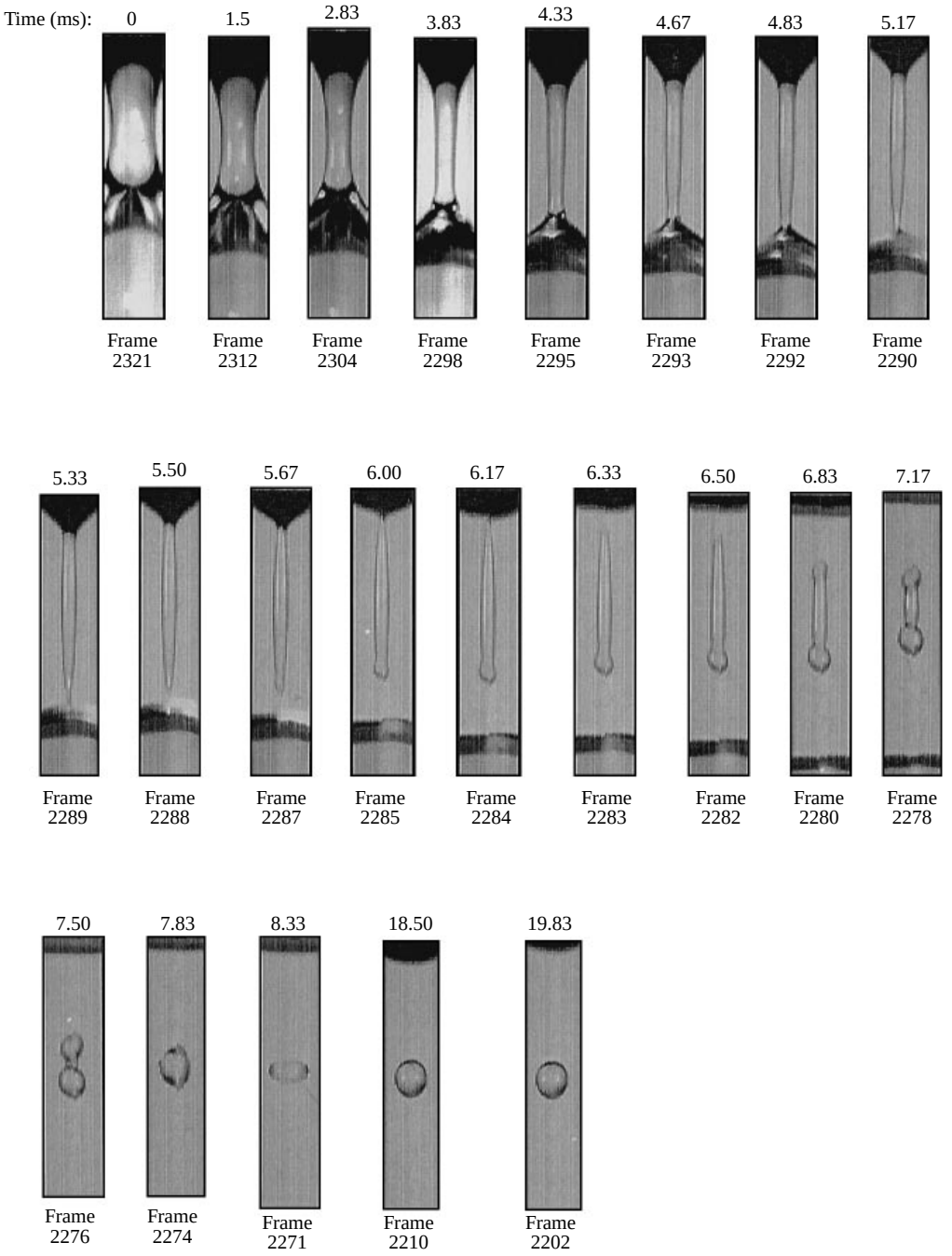

FIGURE 8. Bifurcation and breakage followed at 6000 frames s^{-1}. Bifurcation 0–5.33 ms, breakage 5.33–6.17 ms, followed by satellite drop development. Times are relative to the first frame. Liquid: 80% glycerol in water, viscosity 108 mPa s. Experiment 28/06/95 ID13.

comparing the satellite drop volumes of the same series of experiments as shown in figure 10. All these photos were images captured without any relative change in magnification or size so that all were strictly comparable. Some of these satellite drops were still suffering recoil pulsations and so are not spherical. Even so, it appeared from

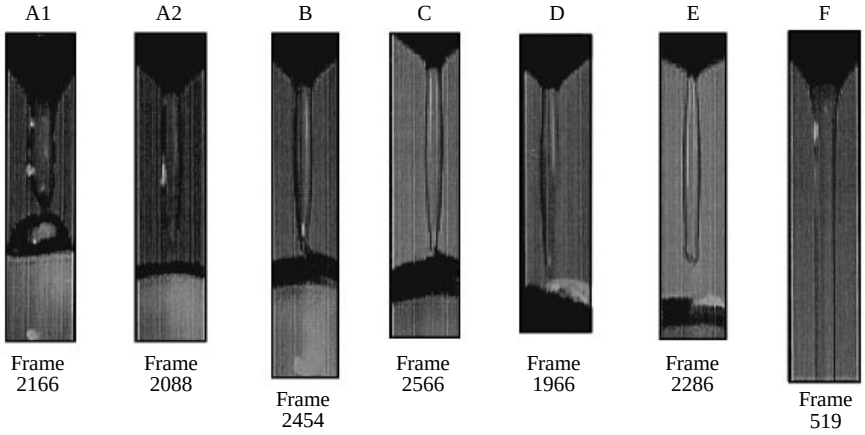

Experiment	Composition	Surface tension	Viscosity
A1 28/6 ID19	Water	72 mN m^{-1}	1 mPa s
A2 28/6 ID20	Water	72	1
B 28/6 ID05	60 % Glycerol	62	14.3
C 28/6 ID12	60 % Glycerol	62	14.3
D 28/6 ID02	70 % Glycerol	62	34.8
E 28/6 ID13	80 % Glycerol	61	108
F 29/6 ID02	Viscoelastic polymer (shear thinning)		650

FIGURE 9. Bridge neck length prior to rupture. All experiments were taken at 6000 frames s^{-1} one frame before rupture.

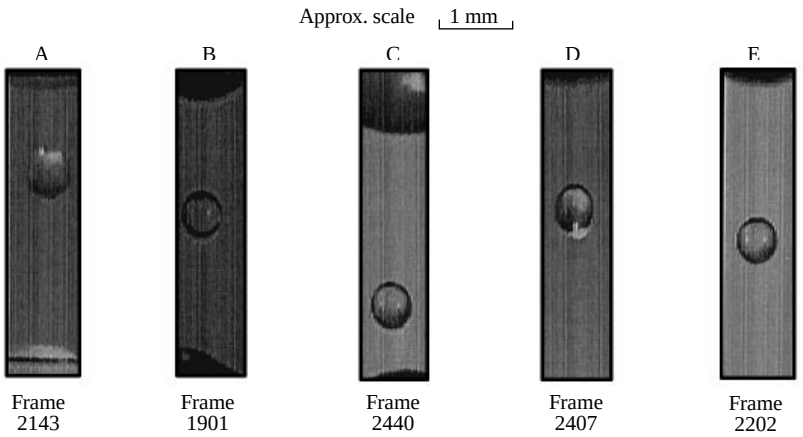

Experiment	Composition	Surface tension	Viscosity
A 28/6 ID19	Water	72 mN m^{-1}	1 mPa s
B 28/6 ID02	70 % Glycerol	62	34.8
C 28/6 ID12	60 % Glycerol	62	14.3
D 28/6 ID05	60 % Glycerol	62	14.3
E 28/6 ID13	80 % Glycerol	61	108

FIGURE 10. Satellite drop size for different liquids. Video frame speed 6000 frames s^{-1} and equal magnifications.

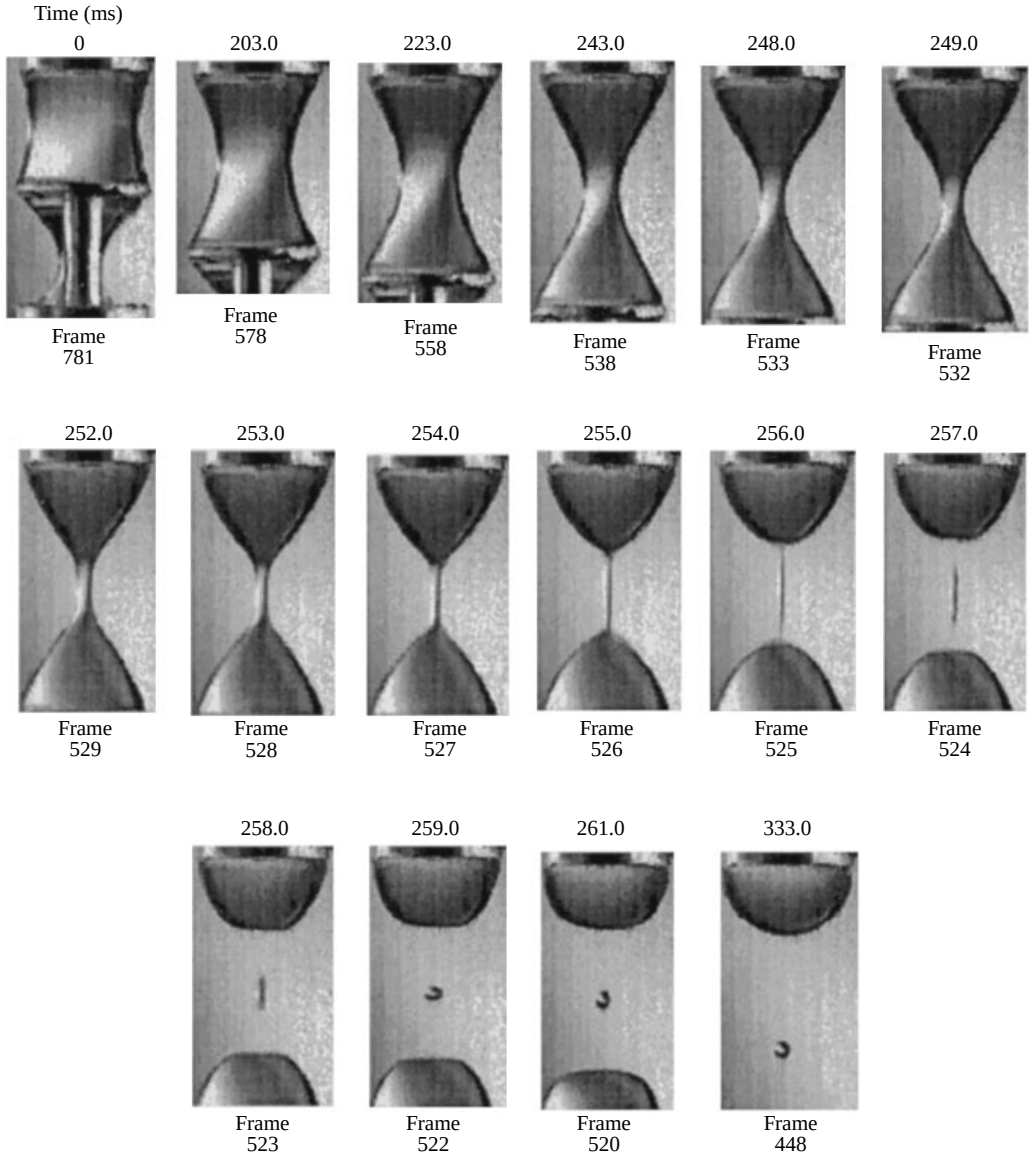

FIGURE 11. Bifurcation and breakage in a plateau tank. Pendant bridge was dioctyl phthalate/dibutyl phthalate mixture in water as the surrounding liquid. Endplates were 4.0 mm diameter and video speed 1000 frames s^{-1}. Experiment 29/06/95, ID05.

these experiments that all satellite drop volumes were about 0.104×10^{-3} mm^3, $\pm 8\,\%$ within the range of viscosities examined.

The neck of the bridge shown in A1 of figure 9 differed from that of A2 in that the pendant endplate was stopped as it was falling away, and before the bridge actually broke. Thus this pendant bridge was transformed into a liquid bridge (figure 1*a*), which broke without satellite drop formation and confirmed a similar experiment with water carried out by Zhang *et al.* (1996).

Figure 9 liquid F shows the neck region of the pendant bridge formed with a very high-viscosity shear thinning liquid. The liquid of this bridge never broke and just extended in the form of a long rod with parallel sides.

7.3. *Breakage in simulated low gravity – Plateau tank experiments*

The liquids – water and a mixture of dibutyl and dioctyl phthalates – and the method for performing Plateau tank experiments have already been described. The purpose here was to determine how breakage took place when the force field was made artificially symmetrical.

In the first experiment, breakage of a floating-endplate pendant bridge was followed at 1000 frames s^{-1} and the sequence is shown in figure 11. Though a small amount of oil phase was split on the lower side of the endplate as seen in the first frame, this should make little difference as the effective weight of the endplate was its weight adjusted to the ratio of its density less that of the surroundings. The bifurcation process proceeded until frame 525 was reached when both ends of the cigar-shaped neck broke simultaneously. In fact, every part of the bifurcation, breakage and recoil took place symmetrically in this experiment.

The first 10 frames of figure 11 indicated that bifurcation took place with both half-zones reaching a near conical shape, as in frame 532, whereas in the gravity field only the liquid at the top endplate reached this characteristic shape, frame 125 of figure 5. The most significant feature of this Plateau tank experiment was that the top and bottom of the neck broke within the same frame (frame 525), even though the lower endplate was accelerating downwards. This suggests that breakage is driven solely by a decrease in surface area of the liquid–fluid interface.

It was found difficult to create a stable long cylindrical pendant bridge with a floating endplate: only short bridges with a neck and no bulge could be formed. Though the computer simulation of pendant bridge growth presented in § 6 has not been attempted for the zero gravity condition, the 1 g simulation suggests that full-length ($\pi 2X_r$) pendant bridges in 0 g would be unstable. Liquid bridge experiments performed in the low-gravity environment of parabolic flight, where one endplate was moved mechanically to stretch the liquid volume beyond its stable length, confirmed this supposition. Accordingly, breakage of a fixed-endplate liquid bridge using the Plateau tank was attempted in order to reach the full Plateau length. Therefore the experiment was set up with a liquid volume greater than that required to form a cylinder (i.e. $V_b > 2(\pi X_r)^2$), the length then fixed at $2\pi X_r$, and the volume now reduced very slowly until the critical volume was reached. The bifurcation and breakage sequence of this experiment was followed at 500 frames s^{-1} and is presented in figure 12.

Frame 762 of figure 12 was regarded as that close to the point of critical instability but before any spontaneous and irreversible shape changes had occurred. The stages of bifurcation and breakage were: first, evolution through a cascade of non-equilibrium Laplace shapes until a cylindrical neck was formed; second, stretching and thinning of the neck until it spontaneously broke at both ends simultaneously; and third, recoil and damping which occurred very rapidly. In this experiment the diameter of the endplates was again 4 mm, and the length of the neck just prior to breaking was relatively shorter than those of pendant bridge experiments with a floating endplate. As the lower plate was not moving in figure 12, the satellite drop stayed in its central position for a very long time as the buoyancy was reduced to zero.

This Plateau tank experiment was unsuccessful in reaching a true cylindrical bridge of maximum length determined by Rayleigh's limiting stability criterion. This failure probably arose because heating from the lighting system appeared to make the oil phase of the bridge somewhat less dense than the water so that a perfect cylinder could not be formed – rather, an amphora shape with a bulge at the upper end and a neck at the lower end of the bridge was obtained. Even so, the sequence of shapes shown in

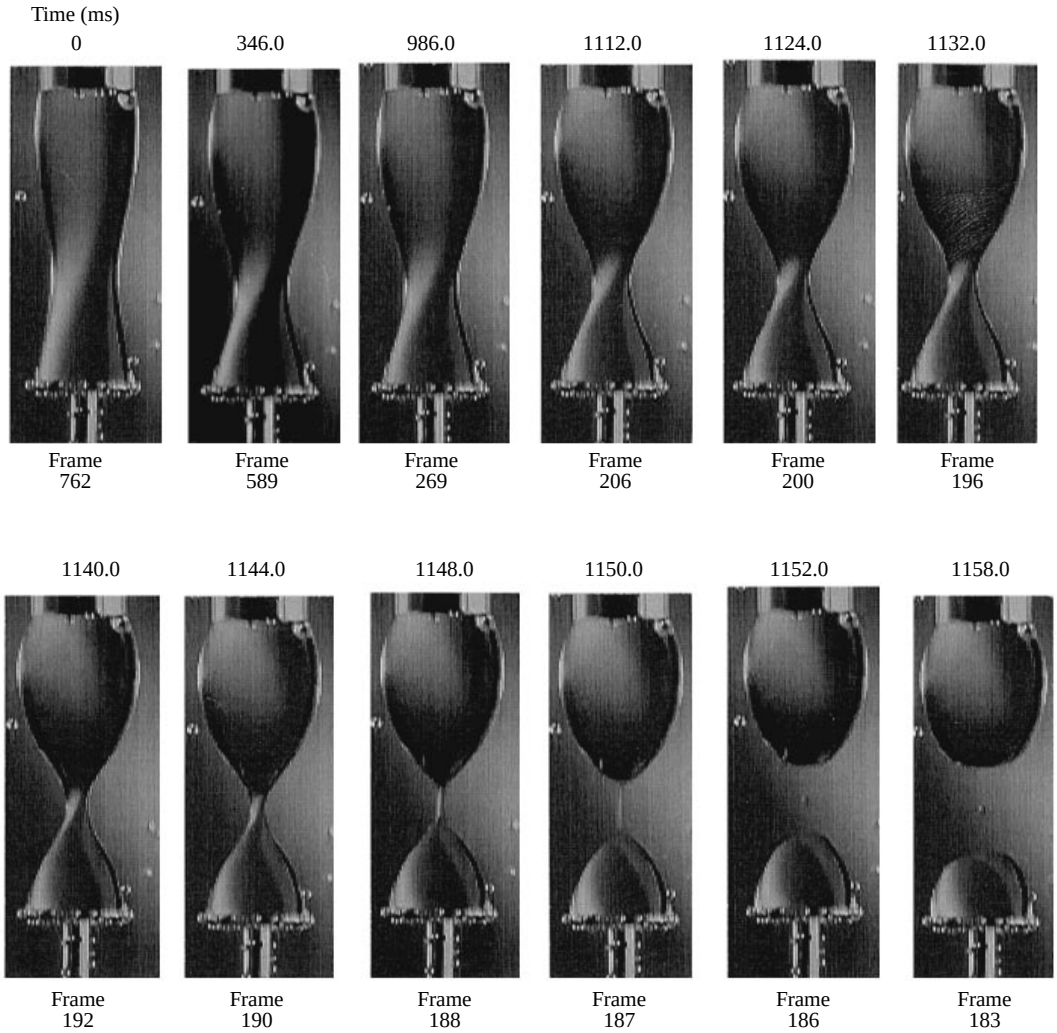

FIGURE 12. Pendant bridge with fixed endplates in a Plateau tank. Bridge liquid was a mixture of dibutyl and dioctyl phthalates and the outer phase was water. Temperature control was very poor due to heating from the strong tungsten lighting. Camera speed 500 frames s^{-1}. Experiment 29/6/95, ID09.

figure 12 demonstrated clearly that breakage of a bridge of fixed length and in a near zero force field appeared to be symmetrical about a plane passing through the centre of the neck region. This symmetry was both in shape and in time. Finally we note that the type of shape created by (i)–(iii) of figure 3, which would be unstable with a pendant bridge, was now stable when endplates were fixed.

8. Conclusions and discussion

This study attempts to describe the processes of growth, bifurcation and breakage of a pendant liquid bridge. The principal properties of the experimental pendant bridges were dimensions taken from their recorded profiles and, where measured, the bridge volume. The evolution of the shape and of associated physical parameters with

time were recorded experimentally using a high-speed camera with digital recording. The growth and stability limit of pendant bridges with differing endplate masses have been simulated by computation from the physical parameters of the system. The shapes of some stable, critical and non-equilibrium liquid bridges were computed using numerical integration techniques and compared with corresponding experiments.

The properties of stable free-floating pendant bridges during growth and up to the point of critical stability have not been studied previously. In this study the modelling of the growth of the bridge has been carried out for systems with endplates of equal diameter. Unequal endplates and those where the wetting is limited by contact angle are all possible but have not been investigated here. Experiments have been limited to one size and mass of the floating endplate.

The dimensionless group, $M/\rho X_r^3$, expressed as V_l/X^3, characterized the growth and stability limit of a pendant bridge system and computed stability limits were in agreement with experiment. For very much smaller values of this dimensionless group the growth of the pendant bridge profile would follow the same pattern but with the floating endplate supported much lower on the pendant drop shape of figure 3. Such bridge profiles would show a bulge near the lower endplate and growth would start at the bulge rather than the neck. When the dimensionless mass ratio of the endplate is very much larger than the value used here, case 3 following equation (16), then the bridge shape would not be represented by a pendant drop profile at all, but would be modelled by the bridge section of a captive sessile bubble which is shown in figure 2(*d*). The position of change-over from pendant drop profile to sessile drop profile would occur when the dimensionless group equals unity, as already described in case 2 following equation (16).

In the early stages of this study it was found that pendant drop tables (Hartland & Hartley 1976) were instrumental in showing that the method would work in principle. The shape tables were used to seek a position within a given table where the cut-off volume of the pendant drop equalled that defined in equation (15). Simple linear interpolation was used for this approximation.

As already noted the comparison of modelled shape with experimental shape could not be made using bridge volume measurements as the volume was changing with time, albeit slowly. Thus we used the ratio Z/X_r as the criterion of comparability between experimental and computed shape. The measuring error of $\pm 2\%$ in Z arose principally from slight distortion of the image which is apparent in figures 6, 7 and 8. Comparison of experimental and computed shape of equal values of Z/X_r, was made using the ratio $2X_n/Z$, in the manner already described.

The growth of the pendant bridge up to and including the critical point of equilibrium was adequately represented by the computer simulation, though refinements might well improve the agreement between modelling and experiment. An interesting feature that emerged from the simulated profiles of figure 7 was that the bridge shape grew from the neck region of a pendant drop profile. For a very much lighter free-floating endplate, the profile would start at the bulge of the drop profile and grow with the later formation of a neck, but always with the bulge present.

The modelling of the non-equilibrium experimental shape such as that of frame 135 in figure 7 by the computed profile (*h*) was, as expected, not very close. As already indicated the neck diameter of the computed bridge was less than that of the experimental bridge whereas it should have been greater if inertia terms were significant. This difference between experiment and calculation was attributed to interpolation of the non-equilibrium volume condition not being met with sufficient accuracy.

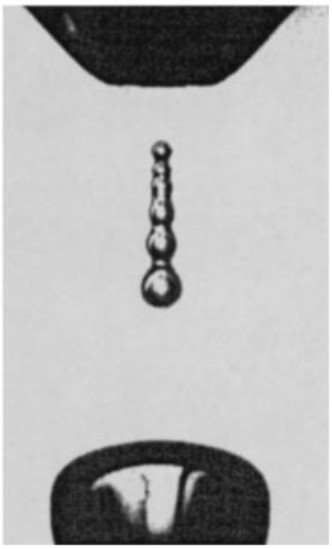

FIGURE 13. High-speed ciné camera image of a pendant drop and its satellite: orifice plate radius, 3.85 mm; orifice material, precision ground glass; liquid, pure distilled water; drop volume falling away, 0.0991 ml; time after breakage of lower end, 2.8 ms; camera speed, 2500 frames s^{-1}.

The bifurcation and ultimate breakage of pendant bridges formed an important experimental part of this study. The time resolution provided by operating at 6000 frames s^{-1} has enabled the point of breakage of each end of the neck of a liquid bridge to be recorded with clarity. We present the visual images of the experiments in time sequence arrays so that the main physical features can be seen clearly. The only experimental uncertainty encountered was the poor temperature control. Temperatures of the liquid bridge were measured before and after breakage with the lighting left on continuously and a rise of at least 10 °C was recorded. To overcome this rise, subsequent experiments were made by introducing liquid into the bridge with the lighting switched off until the bridge was near its stability limit. Further liquid was then introduced with the lights on and after breakage, the lights extinguished again. This procedure reduced the temperature rise to a few degrees only.

The pendant drop data of Peregrine *et al.* (1990), representing a single experiment using water, are compared with the breakages in our figures 5 and 6. Though their lighting and time resolution are superior to our data and provide much better detail of satellite drop development the two data sets are otherwise consistent. Peregrine *et al.* divide up the dynamic development of breakage into three time periods but do not seem to give the same importance to the breakage of the upper region of the neck. Also unpublished high-speed camera images taken by Padday in 1972 of a water drop breaking, a single frame of which is shown in figure 13, confirm Peregrine *et al.*'s (1990) data with remarkable agreement. We believe that the simultaneous breaking of liquid bridges under effective low gravity, shown in figures 11 and 12, with symmetry about a horizontal plane passing through the centre of the neck, denoted the normal situation. It is the external force field of gravity that seems to lead to the planar symmetry of bifurcation and breakage being lost.

As already noted, our data are suitable for comparison with the pendant drop data of Zhang & Basaran (1995) and to a lesser extent to the liquid bridge data of Zhang *et al.* (1996). Zhang & Basaran use the same viscosity range of glycerol/water mixtures

as in this study, and generally we find good agreement with the shapes presented in their figures 1 and 7 for water and for 85 % glycerol respectively. As they do not present their primary data for intermediate concentrations of glycerol in water, comparison with our data of nearly constant neck length and satellite drop size was not possible. However, Padday (1992) demonstrated that, in the low-gravity environment of parabolic flight, breakage of liquid bridges of even higher viscosity, 100 to 200 mPa s, appeared to be entirely different. His liquid bridge was formed with paraffin oil of viscosity of 168 mPa s† and surface tension of 32 mN m^{-1}. Bifurcation was shown to be symmetrical about a plane passing through the centre of the bridge and parallel to the endplates. A neck was formed as expected but with both endplate zones adopting a conical cross-section. Thereafter the neck region never broke, it just stretched and thinned until it disappeared from view with no apparent satellite drop formation. Also it was found that the two half-zones relax into their spherical cap shapes without any recoil or wave formation. We thus conclude that at these much higher viscosities, bifurcation took place with thread formation and no satellite drop, in the manner reported by Padday (1992), Zhang *et al.* (1996), Brenner *et al.* (1994) and Shi *et al.* (1994).

The two experiments in simulated low gravity reported here (figures 11 and 12) were typical of other experiments covering a much wider range of breakages in real low gravity that are being prepared for publication. These latter experiments, like the data of Padday (1990), examined the bifurcation of a very wide range of fixed-endplate liquid bridges and were performed in the controlled environment of parabolic flight (10^{-2} g) and supported the general nature of the Plateau tank experiments reported here. The essential features of these Plateau tank experiments were that first, breakage of a lower-viscosity liquid took place simultaneously at both ends of the neck and secondly the recoiling neck region showed no periodic structure as seen in the figures. We attribute this latter effect to the balance of hydrostatic pressure gradient along the whole length of the neck region. The viscosity of the outer liquid, though water, is nevertheless very much greater than that of air and would enhance damping of any recoil process or wave formation in the neck region. It is noted that the much denser metal floating endplate still exerted a stretching force on the bridge itself even though equal liquid density normalized the hydrostatic pressure within the liquid bridge.

Bifurcation and subsequent breakage were initiated by the surface driven effects accompanied by a decrease in surface energy (i.e. reduction in liquid–air or liquid–liquid surface area), with inertia and viscous terms participating as processes that absorb energy rather than producing it.

Some gravitational stretching took place during the later stages of bifurcation and breakage as seen in figure 5. Thus hydrostatic pressure within the pendant bridge changed by a small amount. Even so the data of figure 6 (frames 2089, 2088 and 2087) and in figure 8 (frames 2093 to 2085) demonstrate that movement of the lower endplate is only just perceptible and that in consequence, gravity potential appeared to play a very small part in the act of breakage of these experiments.

A comparison of our experimental shapes with those predicted by modelling of the bifurcation and breakage process in other investigations was only possible qualitatively, mainly because the modelling studies were not comparable to our experimental procedure and the computer programs by which they were made not available.

Comparison of bifurcation and breakage with the study by Schulkes (1994) provided

† The viscosity of paraffin oil presented in table 1 of Padday (1992) is in error: it should read 168 mPa s.

a good qualitative fit. His modelling experiments were carried out with water forming a pendant drop but which was continuously fed with further water. His figure 4 was derived with a very low discharge rate and predicted a cigar-shaped neck that broke first at the lower end and later at the upper end of the neck region. We have already shown that our breakage volume, like Schulkes' data in his figure 8, is comparable to the data of Padday & Pitt (1973) and therefore that of Harkins & Brown (1919).

Eggers (1995) and Eggers & Dupont (1994) identify the point at which the neck breaks as a singularity in their asymptotic solutions of the Navier–Stokes equation, at which the neck diameter in the region of the break tends to zero. This is clearly indicated in their figure 5 of the 1995 data.

Though the time scale of their model is beyond the resolution of our experiments, we believe that the description agrees with the formation and relaxation of the pimple on the bulk zone which we have seen and recorded many times. Assuming that the surface of the neck outside the 'hot region' must be smooth and continuous, we would have expected a wider neck angle to accommodate the volume of liquid in the neck region that formed the satellite drop. The study by Chacha *et al.* (1995) and that of Papageorgiou (1995) predict a somewhat wider angle which appears to accommodate the satellite drop volume more closely.

A surprising effect of these experiments was that over the viscosity range of liquid forming the pendant bridges they were remarkably similar, suggesting that the capillary number played little part in the breakage process. At first sight this appears inconsistent with the findings of Zhang & Basaran (1995). However, the inconsistency may be due to the quality of the glycerol differing between the two data sets. Glycerol is highly hygroscopic and in our study no attempt was made to determine the water content of the undiluted glycerol. Though their primary data for liquids below 80% glycerol were not presented, their figure 11(*a*) suggests that the breakage length does not vary very much with capillary number. This would be consistent with our findings.

No attempt was made to change the dynamic Weber number by altering the surface tension of the pendant bridge using suitable surfactants in these experiments. Any such use of surfactant would have to ensure that the dynamic surface tension at the short ageing times did not differ from the static value. We note that Zhang & Basaran (1995) use the surfactant Triton X100 to lower the surface tension and then state that 'expansion and stretching of the drop surface occur…'. In our own experiments, especially those in low effective gravity, no expansion of the surface occurred at all. In fact the very reverse occurs: the breakage was totally surface driven and involved a decrease in area of the liquid–air interface of the drop. Thus dynamic surface tension effects would be unlikely to affect the breakage process.

The periodic structure of the neck region once the lower endplate liquid had broken away, as in frames 2084 to 2079 of figure 6 for water, has been examined before (Peregrine *et al.* 1992 and Pétré 1994, unpublished). The transient periodic shape with repeating unduloids could result from the inherited gravitational pressure gradient as shown previously (Padday 1971), from the precursor stage of Rayleigh (1878) instability of a jet, or from an induced wave structure as suggested by Peregrine *et al.* (1990). Figure 13 is an enlarged image of water from the study of Padday (1972), and shows the detail of the structure of the neck region after breaking away. The image corresponds to a time between Peregrine *et al.*'s (1990) images of their figures 8(*a*) and 8(*b*). Though the orifice of Padday's experiment was smaller, the sequence of bulges merging was evident in both experiments. In figure 13 here, the merging of two unduloids (3 and 4) is clearly seen and subsequent merging of further unduloids occurred without loss of shape of the lower bulges. The unduloid merging process

suggests that the waves are unlikely to provide a full explanation of unduloid structure unless their periodic time is several orders of magnitude greater than that of the breakage process.

This study was principally an experimental study supported by some theoretical modelling. Much of the data presented here have taken advantage of modern computer techniques which allowed us to create digitized images of each frame of a video sequence. Thus we were able to follow the bifurcation and breakage of all types of liquid bridges from these images. Such digitized images were readily assembled into the arrays and also easily compared with computed shapes.

This study was carried out within the European Research Board Contract No ERB.CHXT.940481 entitled 'Dynamics of Multiphase Flows across Interfaces'. The computing systems for image processing were supplied under this contract. We thank the CAV of the University of Brussels who put the Kodak High Speed camera at our disposal, and also Mr V. Dery of CAV, for his helpful collaboration.

The authors are indebted to the referees and thank them for stimulating observations on an earlier version and to one of them for calling attention to the recent significant studies of Zhang and Basaran.

Appendix A. Generating equations for use with the computational method for evaluating pendant drop shape and for interpolating pendant bridge properties

(i) Select a fixed value of $M/\rho X_r^3$ obtained from the physical properties of the system defined in the text above. Also select a value of C, the shape factor of the profile to be examined. C must be negative and lie between 0 and -0.6.

(ii) Start the integration at the origin of the pendant drop profile (figure 3). Set values of an array corresponding to X/k, Z/k, F/k, S/k^2, V/k^3 and angle θ equal to zero.

(iii) R_v and R_h, which are equal at the origin, were calculated on the basis that

$$R_v/k = R_h/k = (-1/C)^{1/2}. \tag{A 1}$$

(iv) The distance along the periphery, F/k, was chosen as the independent variable with an increment, $\Delta F/k$, set arbitrarily:

$$\Delta F/k = \mathrm{ABS}(\pi R_v/k)/2000. \tag{A 2}$$

The denominator, 2000, was adjusted to a value derived from error analysis to provide a reproducibility better than $1:10^{-6}$.

(v) Using fourth-order Runge–Kutta, integration was started by inserting the values of X_n/k, Z_n/k and θ_n, for the first round, in the set of equations

$$\Delta\theta_i = (\Delta F/k)\,(Z_o/k - Z/k - \sin\theta_n/X_n), \tag{A 3}$$

$$\Delta X_i/k = (\Delta F/k)\cos\theta_n, \tag{A 4}$$

$$\Delta Z_i/k = (\Delta F/k)\sin\theta_n, \tag{A 5}$$

$$\Delta S_i/k^2 = 2\pi(X_n/k)\,\Delta F/k \tag{A 6}$$

$$\Delta V_i/k^3 = (\Delta F/k)\sin\theta_n)\,\pi(X_n/k)^2. \tag{A 7}$$

(vi) Second-, third- and fourth-round elements of the increments were now calculated successively in the usual way.

(vii) The weighted increment for each property was now found using all four elements in

$$P_{n+1} = P_n(\Delta P_{\mathrm{i}} + 2\Delta P_{\mathrm{ii}} + 2\Delta P_{\mathrm{iii}} + \Delta P_{\mathrm{iv}})/6 \tag{A 8}$$

and when calculated added to the stored values of each parameter.

(viii) As increments of $\Delta F/k$ were rarely if ever wanted, though they were mathematically very convenient to use, it was necessary to adapt this procedure in order to locate exact positions on the periphery where the angle θ, the horizontal radius X/k, the volume V/k^3, or any other property reached some predetermined value. The methods used were not very different and are as follows.

(ix) A predetermined value of X_r/k: the Runge–Kutta integration was continued until the desired value of X/k, was passed. Equations (A 1)–(A 7) were replaced with the following sequence:

$$\Delta(X_n/k) = X_r/k - X_n/k, \tag{A 9}$$

$$R_v/k = (-1/C)^{1/2} - Z_n/k - k(\sin\theta_n)/X_n, \tag{A 10}$$

$$\phi_n = \arccos(-\Delta(X_n/k)/(R_v/k)), \tag{A 11}$$

$$\Delta F/k = (R_v/k)(\phi_n - \theta_n)\pi/180, \tag{A 12}$$

where X_n/k was the value of X/k that exceeded the desired value. With this newly derived value of $\Delta F/k$, steps (v) and (vi) were now carried out sequentially which provided the exact fit to the required value of X_r/k.

(x) A predetermined value of angle θ_r: equations (A 1) and (A 3) were replaced by the sequence:

$$\Delta\theta_n = \theta_r - \theta_n, \tag{A 13}$$

$$R_v/k = (-1/C)^{1/2} - Z_n/k - k\sin\theta_n/X_n, \tag{A 14}$$

$$\Delta F/k = \Delta\theta_n(\pi/180)(X_n^2/k^2)\,R_v/k. \tag{A 15}$$

With this newly derived value of $\Delta F/k$, steps (v) and (vi) were now carried out sequentially but omitting equation (A 3), to provide an exact fit to the required value of θ_r.

(xi) The procedure for extracting a point on a profile at which V_l/X_r^3 equals $M/\rho X_r^3$, involved monitoring the value of V/X^3 until it exceeded the fixed value being sought. As both V and X are changing, the increment was derived on the basis of differentiating the expression by parts and then rearranging the equation to provide an expression for the increment $\Delta(X_n/k)$ as set out in the next step.

(xii) A predetermined value of angle V_l/X_r^3 $(= M/\rho X_r^3)$: equation (A 1) was replaced with the following:

$$\Delta(V_n/X_n^3) = V_l/X_r^3 - V_n/X_n^3 \tag{A 16}$$

$$\mathrm{d}v\,\mathrm{d}x = (V_n - V_{n-1})/(X_n - X_{n-1}), \tag{A 17}$$

$$\Delta(X_n/k) = \Delta(V_n/X_n^3)/(\mathrm{d}v\,\mathrm{d}x/X_n^3 - 3(V_n/X_n^4)). \tag{A 18}$$

Then proceed with the increment $(\Delta(X_n/k))$ using (k) and (A 10), (A 11) and (A 12).

REFERENCES

Bashforth, F. & Adams, J. C. 1883 *An Attempt to Test the Theories of Capillary Attraction*. Cambridge University Press.

Bouasse, H. 1922 *Capillarité, Phénomènes Superficiels*, Chap. 6, 7. Delagrave Paris.

Brenner, M. P., Shi, X. D. & Nagel, S. R. 1994 Iterated instabilities during drop formation. *Phys. Rev. Lett.* **73**, 3391.

Chacha, M., Occelli, R., Tadrist, L. & Radev, S. 1995 Numerical treatment of the instability and the breakup of a liquid capillary column in a bounded immiscible phase. *Intl J. Multiphase Flow 1997*, vol. 23, pp. 377–395.

Edgerton, H. E., Hauser, E. A. & Tucker, W. B. 1937 *J. Phys. Chem.* **41**, 1017–1028.

Eggers, J. 1995 Theory of drop formation. *Phys. Fluids* **7**, 941–953.

Eggers, J. & Dupont, T. F. 1994 Drop formation in a one-dimensional approximation of the Navier–Stokes equation. *J. Fluid Mech.* **262**, 205.

Harkins, W. D. & Brown, F. E. 1919 The determination of surface tension and the weight of a falling drop: the surface tension of water and benzene by the capillary height method. *J. Am. Chem. Soc.* **41**, 499–524.

Hartland, S. & Hartley, R. W. 1976 *Axisymmetric Fluid–Liquid interfaces*. Elsevier.

Huh, C. & Scriven, L. E. 1969 Shapes of axisymmetric fluid interfaces of unbounded extent. *J. Colloid Interface Sci.* **30**, 323.

Keller, J. B. & Miksis, M. J. 1983 Surface tension driven flows. *SIAM J. Appl. Maths* **43**, 268–277.

Meseguer, J. 1983 The breaking of axisymmetric slender liquid bridges. *J. Fluid Mech.* **130**, 123–151.

Meseguer, J. & Sanz, A. 1985 Numerical and experimental study of the dynamics of axisymmetric liquid bridges. *J. Fluid Mech.* **153**, 83–101.

Padday, J. F. 1963 Heights of sessile drops and meniscus properties. *Nature* **198**, 378–379.

Padday, J. F. 1971 The profiles of axially symmetric menisci. *Phil. Trans R. Soc. Lond.* **269**, 265–293.

Padday, J. F. 1992 The formation and breakage of liquid bridges under microgravity. *Microgravity Q.* **2**, 239–249.

Padday, J. F. & Pitt, A. R. 1972 Axisymmetric meniscus profiles. *J. Colloid Interface Sci.* **38**, 323–334.

Padday, J. F. & Pitt, A. R. 1973 The stability of axisymmetric menisci. *Phil. Trans R. Soc. Lond.* **275**, 489–528.

Padday, J. F., Pitt, A. R. & Pashley, R. M. 1975 Menisci at a free liquid surface: surface tension from the maximum pull on a rod. *J. Chem. Soc. Farad. Trans. I.* **71**, 1919–1931.

Papageorgiou, D. T. 1995 Analytical description of the breakup of liquid jets. *J. Fluid Mech.* **301**, 109–132.

Peregrine, D. H., Shoker, G. & Symon, A. 1990 The bifurcation of liquid bridges. *J. Fluid Mech.* **212**, 25–39.

Pétré, G. 1995 Liquid bridge methods for interfacial tension determination. Unpublished report.

Pétré, G. & Wozniak, G. 1986*a* Shape of a liquid bridge and interfacial tension. *Adv. Space Res.* **6**, 133.

Pétré, G. & Wozniak, G. 1986*b* Measurement of the variation of interfacial tension with temperature between immiscible liquids of equal density. *Acta Astronautica* **13**, 669.

Plateau, J. 1873 *Statique Expérimentale et Théorique des Liquides soumis aux seules Forces Moléculaires*, Vol. I, Chap. 2, pp. 66–78. Gautier-Villars Paris.

Rayleigh, Lord 1878 Instability of jets. *Proc. Lond. Math. Soc.* **10**, 4.

Rayleigh, Lord 1880 On the stability of certain fluid motions. *Proc. Lond. Math. Soc.* **10**, 57–70.

Schulkes, R. M. S. M. 1994 The evolution and bifurcation of a pendant drop. *J. Fluid Mech.* **278**, 83–100.

Shi, D., Brenner, M. P. & Nagel, S. R. 1994 A cascade of structure in a drop falling from a faucet. *Science* **265**, 219–222.

Wilson, S. D. R. 1988 The slow dripping of a viscous fluid. *J. Fluid Mech.* **190**, 561–570.

Wozniak, G., Pétré, G., Siekmann, J. & Zumbach, F. 1993 Konstruktion und Erprobung einer neuartigen Apparatur zur Messung von Grenzflächenspannungen zwischen Fluiden. *Engng Res.* **59**, 37–41.

Zhang, X. & Basaran, O. A. 1995 An experimental study of dynamics of drop formation. *Phys. Fluids* **7**, 1184–1203.

Zhang, X., Padgett, R. S. & Basaran, O. A. 1996 Nonlinear deformation and breakup of stretching liquid bridges. *J. Fluid Mech.* **329**, 207–245.